554 *Chem. Mater.* **2011,** *23,* 554–567
DOI:10.1021/cm102252w

CHEMISTRY OF MATERIALS
Review

Charge-Carrier Transporting Graphene-Type Molecules†

Wojciech Pisula,‡ Xinliang Feng, and Klaus Müllen*

Max Planck Institute for Polymer Research Ackermannweg 10, D-55128, Mainz, Germany.
‡Present address: Evonik Degussa GmbH, Process Technology & Engineering, Process Technology−New Processes, Rodenbacher Chaussee 4, 63457 Hanau-Wolfgang, Germany

Received August 8, 2010. Revised Manuscript Received October 5, 2010

Graphene-type molecules, typically large polycyclic aromatic hydrocarbons (PAHs), have gained enormous interest because of their unique self-organization behavior and promising electronic properties for applications in organic electronics. This article reviews the thermotropic behavior and supramolecular organization of discotic PAHs in the bulk as well as their self-assembly on the surface at different length scales. Applications of PAHs in field-effect transistors and solar cells are discussed in light of various different processing approaches from solution that ensure high order and an adequate molecular arrangement in the device configuration.

1. Introduction

Since the discovery of the organic photovoltaic cell,[1] light-emitting diode (LED),[2] and field-effect transistor (FET)[3] in the mid 1980s, interest in organic electronic devices has steadily increased in both academic and industrial institutions. Such devices are expected to be ultimately incorporated, for instance, into all-plastic integrated circuits for low-end and cheap electronics and all-plastic light-emitting displays, where each pixel consists of an organic LED driven by an organic FET.[4] In all of these applications, the efficiency of charge carrier transport through the organic layer(s) plays a key role in the final device performance. In organic FETs, it is desirable to develop new materials displaying high electron and hole mobilities with the aim to design complex organic circuits.[5] In organic photovoltaic cells, the charges created upon photoexcitation of the active components have to be transported efficiently to be collected at the metallic electrodes with the avoidance of charge recombination at the organic donor/acceptor interfaces.[6] Along these lines, organic chemists have pursued various π-conjugated systems as active materials for electronic devices.[7] The charge-carrier transport properties critically rely not only on the intrinsic electronic properties of the materials but also on the microscopic and macroscopic order of the molecules in solid state.[8] In this regard, the control of molecular organization with long-range ordering on surface through the chemical design and physical processing constitute key aspects in electronic devices.[9]

Among various widely investigated conjugated molecules in organic electronics, conjugated discotic materials represent an intriguing system because of their unique liquid crystalline properties.[10,11] It is well-established that molecules forming discotic mesophases are typically made of a central rigid discotic conjugated core substituted by flexible substituents. The liquid crystallinity originates from the microphase segregation of the two constituents: the crystalline character is promoted by the interaction between the conjugated cores while the liquid character results from the melting of the saturated alkyl chains in the mesophase.[12] Discotic molecules organize spontaneously into one-dimensional columnar suprastructures, which can be oriented by external fields and possess self-healing properties, i.e., the capability of repairing structural defects upon thermal annealing in contrast to crystalline materials. The aromatic components in the columnar suprastructure can serve as important media for one-dimensional electron transport. The search for discotics is, however, mostly ruled by empirism since subtle changes in the number, size, and nature of the lateral chains can lead to unpredictable evolutions of the thermotropic properties and finally influence their electronic properties in devices. In recent years, extensive research efforts have been paid to the discotic system with expanded aromatic cores.[13] It has been recognized that larger aromatic cores can lead to discotic liquid crystals with enhanced columnar stability and high supramolecular order and thus to materials with improved charge-transport property resulting from a more extended π-orbital overlap.

Polycyclic aromatic hydrocarbons (PAHs), belonging to the family of discotics that are also termed nanographenes with an average diameter smaller than 10 nm, can be regarded as two-dimensional graphene segments composed of all-sp^2 carbons. These graphene-type molecules hold advantages over other graphene materials (graphene sheet and graphene nanoribbon) in terms of structural perfection, production scale and physical processability. The typical synthesis of these extended PAHs can be based on the intramolecular cyclodehydrogenation and planarization of 3D dendritic or hyperbranched polyphenylene precursors.[14] By employing this concept, all kinds of large benzenoid PAHs with different molecular sizes,

† Accepted as part of the "Special Issue on π-Functional Materials".

*Corresponding author. Fax: (+49) 6131-379-350. Tel: (+49) 6131-379-150. E-mail: muellen@mpip-mainz.mpg.de.

 Published on Web 10/26/2010

Chart 1. Chemical Structures of Several Large PAHs

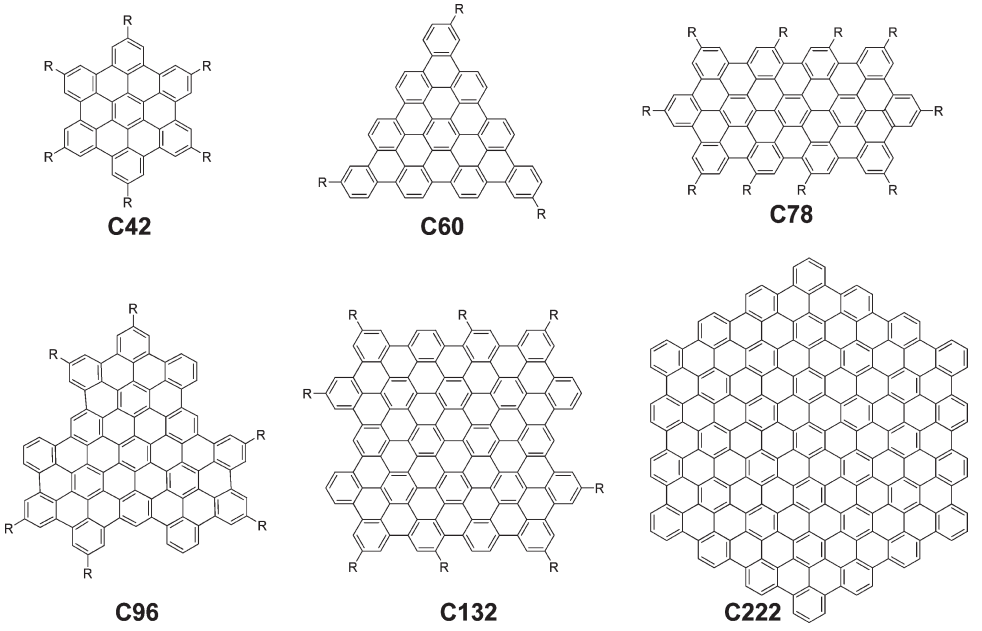

symmetries and peripheries have been made available (Chart 1). Up to now, the largest graphene-type molecule with disk shape consisting of 222 carbon atoms is accessible.[15] Other large PAHs with e.g. triangle-shape (C60),[16] linear ribbon-shape (C78),[17] cordate-shape (C96),[18] square-shape (C132), and others are also attainable. Hexa-*peri*-hexabenzocoronene (HBC, C42), with 42 carbon numbers, is one of the most extensively studied discotic graphene-type molecule. So far, a local charge carrier mobility as high as 1.1 cm^2/vs has been determined for HBC by means of PR-TRMC (pulse-radiolysis time-resolved microwave conductivity) technique.[19] This has stimulated the incorporation of these distinctive materials in electronic devices including organic solar cells and FETs.

It is clear that a successful fabrication of high-performance optoelectronic devices based on discotic graphene materials requires a fundamental understanding of the mechanism of the charge carrier transport within the active layer. This review article discusses several aspects which have a great effect on the migration of charge carriers at different length scales: local (few nanometers), mesoscopic (several hundred nanometers up to few micrometers), and macroscopic (bulk). We first give a brief overview over the thermotropic behavior and the supramolecular organization of PAHs in the bulk state and the influence of the molecular packing in different phases on the transport. The processes at the mesoscopic range are presented in terms of the formation of nanofibers and -tubes and their transfer into electronic devices. In the last part, the focus is on the processing of PAH molecules into thin films that control molecular order and macroscopic alignment of columnar structures for field effect transistors and solar cells.

2. Supramolecular Organization in the Bulk State

The bulk organization and the phase formation are ruled by the shape and size of the aromatic core and the geometry of the attached aliphatic side chains. In the bulk, the substituted molecules arrange in well-defined supramolecular architectures. Since the columnar self-assembly of thermotropic discotic liquid crystals has been already described in great detail in other reviews,[10,11] only a brief overview will be given here.

The molecules stack on top of each other in columns due to π-stacking interactions between individual aromatic cores and due to a local nanophase separation between the rigid core and the surrounding flexible aliphatic side chains. This organization is well described by a model taking into account the density of graphite inside the columns (2.25 g/cm^3), and the density of low molecular polyethylene for the alkyl side chains (0.9 g/cm^3).[20] The calculated intercolumnar spacing based on this model is in good accordance to experimental results from X-ray scattering for molecules with different core sizes (Figure 1).

The thermal behavior of the PAHs is controlled by the variation of the length and bulkiness of the flexible aliphatic side chains attached to the aromatic disk. More bulky substituents, such as long and branched chains, decrease the phase transition temperatures significantly. On the other hand, larger aromatic cores enhance the π-interactions leading to a close packing distance between neighboring discs and to a stabilization of the columnar arrangement. Simultaneously, the phase transition temperatures increase. Even closer molecular packing and improved columnar stability are obtained when small rigid phenyl units are located at the core proximity[21,22] or functional groups for additional noncovalent forces like hydrogen bonding,[23,24] and dipole−dipole interactions[25,26] are introduced. Such functionalization is a powerful tool for achieving control over the columnar organization of PAHs. Thereby, three main phases can be established: crystalline, liquid crystalline, and isotropic phase. The states differ in molecular dynamics and arrangement. Although a high overall order is present in the crystalline phase,[27] in the intermediate liquid crystalline state the discs undergo lateral

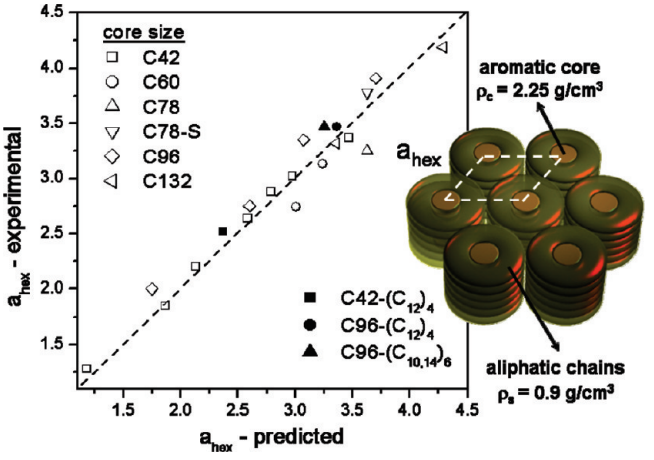

Figure 1. Hexagonal unit-cell parameters obtained from experiments and theory are in close agreement. The model is based on the densities of graphite and low molecular polyethylene, which describe the aromatic fraction and the peripheral side chains. The unit cell of PAHs with aromatic cores consisting from 42 up to 132 carbon atoms and substituted by side chains of various lengths is presented. Adapted with permission from ref [20]. Copyright 2005 American Chemical Society..

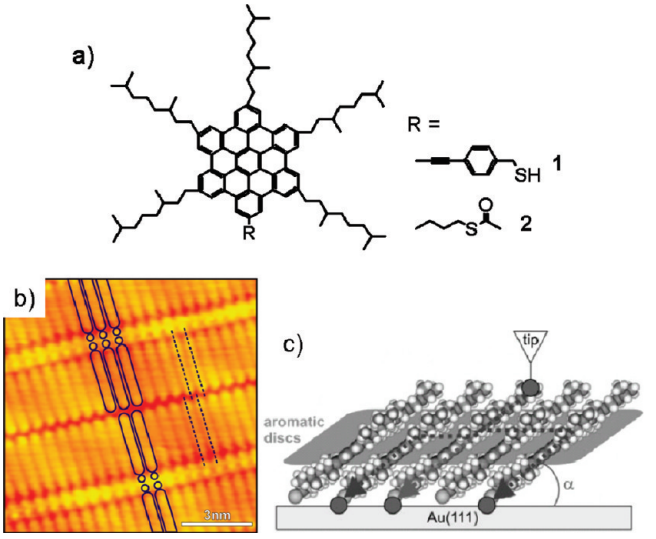

Figure 2. (a) HBC derivatives with attached thiol groups, (b) STM image of **1** on Au/mica, (c) schematic illustration of the molecular transport process by including also lateral transport to neighboring molecules. Reprinted with permission from ref [32]. Copyright 2010 Wiley-VCH Verlag GmbH & Co. KGaA.

and longitudinal fluctuations.[28] This phase allows a spontaneous self-healing of structural defects and grain boundaries leading to a monodomain and finally to an improved charge-carrier transport.[29]

3. Charge-Carrier Transport along One-Dimensional Stacks

The charge migration along the columnar structures has a one-dimensional character and takes places because of extensive interactions between the π-orbitals of adjacent aromatic cores in which the electrons are delocalized. The one-dimensionality is due to the insulation of the conducting pathway by peripheral long aliphatic hydrocarbon chains as schematically illustrated in Figure 3. The charge-transport mechanism is explained by a hopping of the charge carries between neighboring molecules, but for high-mobility systems a degree of band-structure development is assumed.[30] There is a significant discrepancy between intrinsic and extrinsic charge carrier transport. For instance, the pulse-radiolysis time-resolved microwave conductivity (PR-TRMC) method provides valuable information about the intrinsic (local) transport mechanism in discotic liquid crystalline materials.[31] The derived charge carrier mobility is an estimated value on a nanometer length scale because interface effects caused by electrodes are avoided and electric field effects are minimized. Structural defects and impurities acting as charge carrier traps can be neglected. The measurements are performed on simple powder, because the orientation of the molecules and the columnar stacks does not influence the result. In surface layers the effect on the intrinsic electrical properties is different and can be investigated together with the structural quality by employing scanning tunneling microscopy (STM).[32] For this, HBC-thiolates (Figure 2a, **1** and **2**) are deposited as ultrathin films on a gold surface at which the molecules are anchored through covalent S−Au bonds.[32] High-resolution STM images depict highly ordered parallel lamellae aligned along the substrate high-symmetry direction in which the molecules are tightly packed and are tilted toward the substrate by 37−38° (Figure 2b,c). For compound **2**, a HBC core−core distance of only 0.31 nm is measured. To gain insight into the electronic behavior of the thin layer, the local tunneling resistance at different temperatures is determined for islands of **1** and **2** embedded in an insulating, 2D matrix of decanethiolates. Because of the high lateral order and close intermolecular distance, electron mobilities on the order of 5 $cm^2/(V\,s)$ at 28 °C are estimated. This is currently the highest intrinsic value for a HBC carrying alkyl side chains. Additional temperature-dependent measurements give strong evidence for a bandlike transport of electrons.

In great contrast to time-of-flight (TOF)[33,34] or FET measurements, intrinsic mobilities estimated from PR-TRMC or STM are typically few orders of magnitude higher and represent only the local behavior of the material. For the TOF experiment, the sample is sandwiched between two electrodes and a pulsed laser creates the mobile charge carriers in the material that drift under an external electric field over a defined distance (from one electrode to the opposite one).[35] The mobility is extracted directly from drift time, E-field, and distance. Additionally, the shape of the recorded transient plot allows a distinction between a dispersive and nondispersive charge carrier transport. The transport mechanism is highly sensitive to the molecular orientation of discotic PAHs toward the electrodes (this issue is discussed in great detail in section 5), defect density, grain boundaries, and structural order. The same effect is true for FET devices in which these macroscopic traps lower the electronic performance. Only in a few cases (single crystals are excluded) is it possible to reach the maximum intrinsic values for macroscopically aligned samples.[36,37]

The charge hopping between neighboring π-stacked aromatic molecules is less efficient than the charge transfer along an ideal conjugated system, e.g., a conjugated polymer

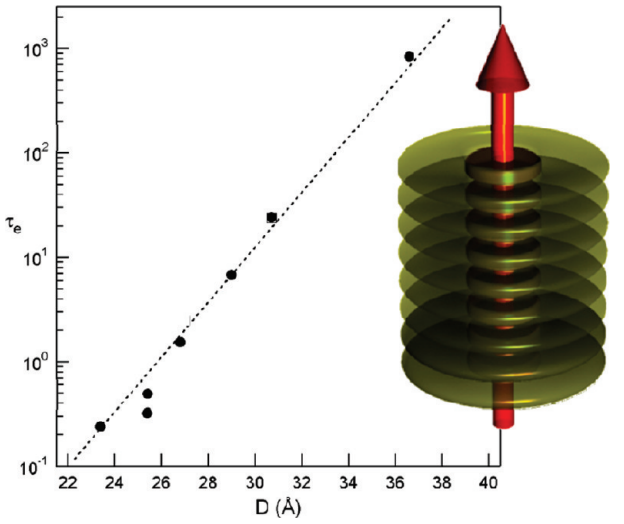

Figure 3. Relation between the exponential conductivity decay time and the calculated disk diameter, *D*, for hexa-alkyl substituted HBCs (inset: illustration of a single one-dimensional pathway for charge carriers which migrate along the stacked conductive graphene-like molecules). Adapted with permission from ref [45]. Copyright 2005 American Chemical Society.

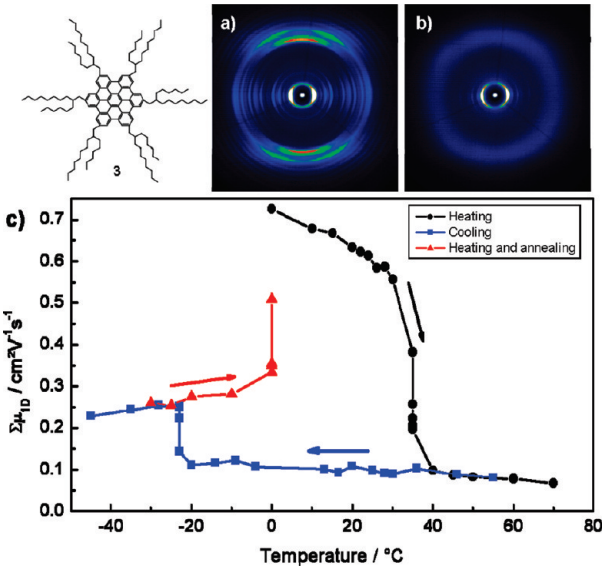

Figure 4. 2D WAXS patterns of **3** determined for (a) 20 °C and (b) 60 °C, (c) PR-TRMC mobility recorded during a heating/cooling cycle for **3**. Adapted with permission from ref [47]. Copyright 2006 American Chemical Society.

backbone.[38] The high room temperature mobilities of approximately 5 cm^2/(V s) for HBCs are assumed as an upper limit for noncovalently bonded molecules and are attributed to their pronounced self-organization propensity into highly ordered supramolecular structures.[32] Significantly higher charge-carrier mobility was found for discotic systems with larger aromatic core sizes.[39,19] This phenomenon was related to an increased π-orbital overlapping for extended nanographene discs.[40] The π-orbital overlap can be further improved through an optimization of the rotation angle between neighboring molecules within the one-dimensional stack. This optimized angle depends on the π-conjugated disk symmetry and size as indicated by calculations based on Marcus theory.[41] To ensure a fast charge carrier transport, the rotation angle can be modified through the molecular symmetry,[42] the attachment of rigid substituents,[43,44] or supplementary noncovalent interactions.[25,26]

Recombination and trapping of charge carriers are the main limiting factors that reduce the final device performance. The lifetime of charge carriers of HBC derivatives is a function of the thickness of the insulating alkyl mantel and is attributed to the intercolumnar tunneling and recombination of charge carriers through the intervening aliphatic hydrocarbon chains.[45] The lifetime rises a few orders of magnitude when the alkyl chain length is extended from 8 to 24 carbon atoms corresponding to a disk diameter increase from 2.4 to 3.7 nm (Figure 3). Even significantly longer lifetimes are obtained for HBCs with ester−ether groups included into the paraffinic side chains.[46]

Trapping of charge carriers occurs due to inorganic impurities, structural imperfection in the crystal and disorder in the organization. Especially the molecular packing and intracolumnar order of discotic PAHs have a strong impact on the mobility of charge carriers. Highly ordered crystalline phases show the highest local mobility values, whereas less ordered liquid crystalline states result in decreased performance.[47] The charge-carrier migration can even collapse if the molecules are disordered within the columns (see example in Figure 4). Simulations give a good insight into the relation between substitution and the molecular packing or the charge carrier transport.[48] Thereby, different approaches can be combined to achieve a detailed theoretical picture for the system.[49] Molecular electronic structures and reorganization energies are determined on the basis of quantum chemical methods. Additionally, kinetic Monte Carlo simulations are used for the charge transport, while molecular dynamics are applied for simulation of the relative positions and orientations of molecules in the columnar mesophase.

4. Fiber Growth and Their Electronic Applications

Solution processing of alkylated PAHs is essential for their application as organic semiconductors in field-effect transistors and photovoltaic cells in which the self-assembly of the molecules takes place on the surface. Macroscopic order and film morphology, which affect the device performance to a great extent, are strongly influenced by the processing conditions including concentration, temperature, type of solvent, and surface treatment. Sound understanding of the assembly mechanism and organization process during solidification from solution is required to gain an optimized morphology. It is also important to be aware of the initial stage of the assembly taking place already in solution before the deposition from solution. Additionally, the molecular architecture such as geometry and type of substituents, size and shape of the aromatic core play also a considerable role on the morphology during device fabrication. The thermal behavior and solubility can be well-controlled by the right choice of the substituents by adjusting the molecular noncovalent interactions through the peripheral steric demand. As presented in Figure 5, concentration-dependent ^{1}H NMR studies for HBC derivatives **4** and **5** reveal that alkyl side chains differing in their length and degree of branching

show marked effects on the self-association in solution.[50] This result indicates that the HBC with bulky, branched side chains (**5**) aggregates at a much higher concentration in comparison to the derivative **4** with only linear alkyls. This discrepancy in solution aggregation is quantified by the self-association constant K_a which is significantly higher for **4**. Because of the stronger aggregation, **4** assembles into distinct one-dimensional fibers during spin-coating from a diluted solution, whereas poor molecular interactions of **5** lead to randomly distributed nanometer-sized blobs (AFM insets in Figure 5).

The fiber growth is a kinetically driven process that can be well-controlled by the processing conditions like changing the evaporation rate of the solvent. The kinetic aspect is especially distinct for PAHs such as **6** carrying short, but bulky side chains. Short crystalline objects appear after drop-casting compound **6** from THF (Figure 6a), but hundreds of micrometer long fibers grow when a high boiling solvent is used. For such kinetically sensitive aggregation, an adequate processing method has to be identified. In the case of **6**, it was found that the slow processing by dip-coating can yield highly oriented thin layers.[50] This technique was also successfully applied for the orientation of conjugated copolymer and small oligomers.[51,52]

Introducing functional groups for additional noncovalent forces at the aromatic core or at the side chains assists the π-stacking interactions of alkylated PAHs and favors the self-organization into even more complex nanosized structures.[53] Such intermolecular forces can originate from hydrogen bonds, dipole- or ionic-interactions. For instance, compounds **7** and **8** possess local dipoles that significantly improve the bulk organization and lead to well-defined nanofibers after solution deposition. Several-micrometer-long and ca. 100 nm wide fibrous structures are observed for **7** from a THF/methanol solvent mixture and consist of dozens of bundles of stacked molecular wires oriented along the fibers.[25] UV/vis and fluorescence indicate indeed a pronounced aggregation in this solvent mixture which is attributed to local dipoles. The deposition of **8** from various solvents displays in all cases a similar morphology consisting of a fibrous network with 500 nm thick fibers with lengths up to few hundred micrometers (Figure 7c).[26] These

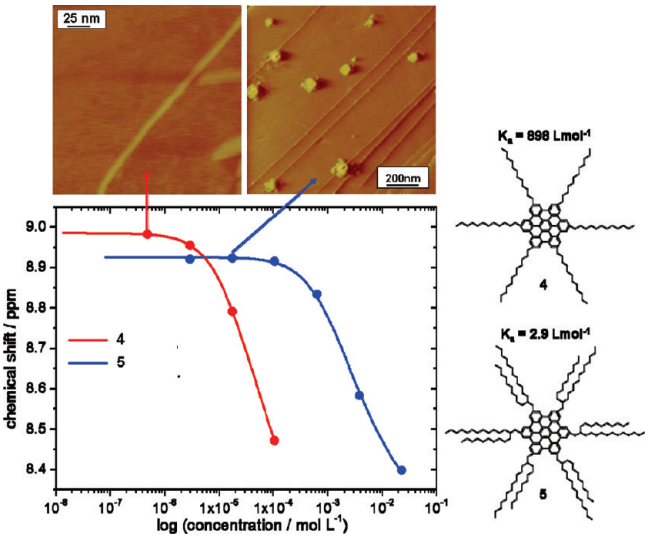

Figure 5. Concentration-dependent ^{1}H NMR chemical shifts of **4** and **5** recorded in 1,1,2,2-tetrachloroethane-d_2 (30 °C, 500 MHz) and fitted with the infinite self-association model including next-nearest-neighbor relations. AFM topologies are shown for spin-coated films. Association constants K_a for self-aggregation of **4** and **5** are determined in 1,1,2,2-tetrachloroethane-d_2 at 30 °C. Adapted with permission from ref [50]. Copyright 2005 American Chemical Society.

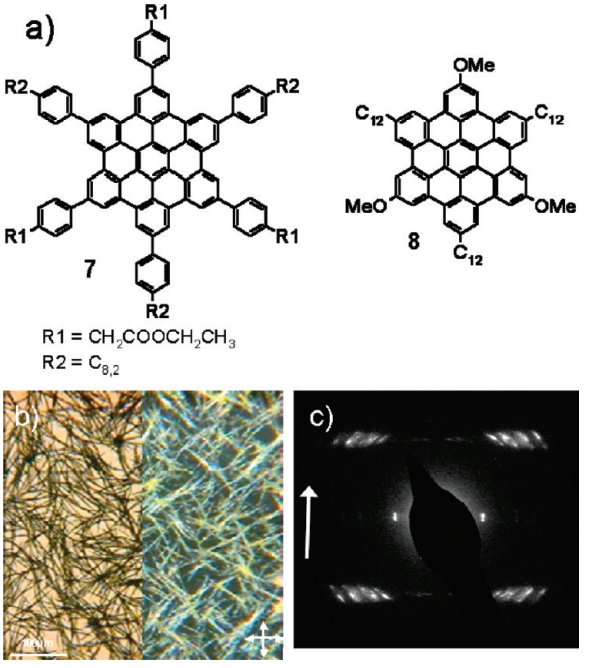

Figure 7. (a) PAHs **7** and **8** possessing local dipoles, (b) optical microscopy image of **8**, (c) electron diffraction pattern of a single fiber of **8**. Adapted with permission from ref [26]. Copyright 2008 American Chemical Society.

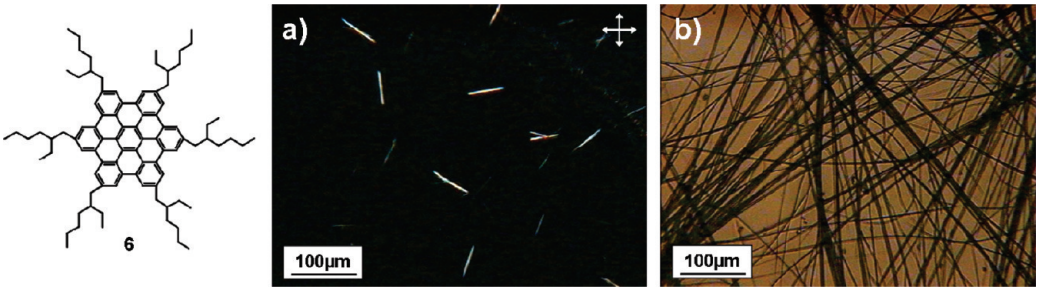

Figure 6. Polarized optical microscopy (POM) images of **6** drop-cast from a solvent with (a) low and (b) high boiling point. Adapted with permission from ref [50]. Copyright 2005 American Chemical Society.

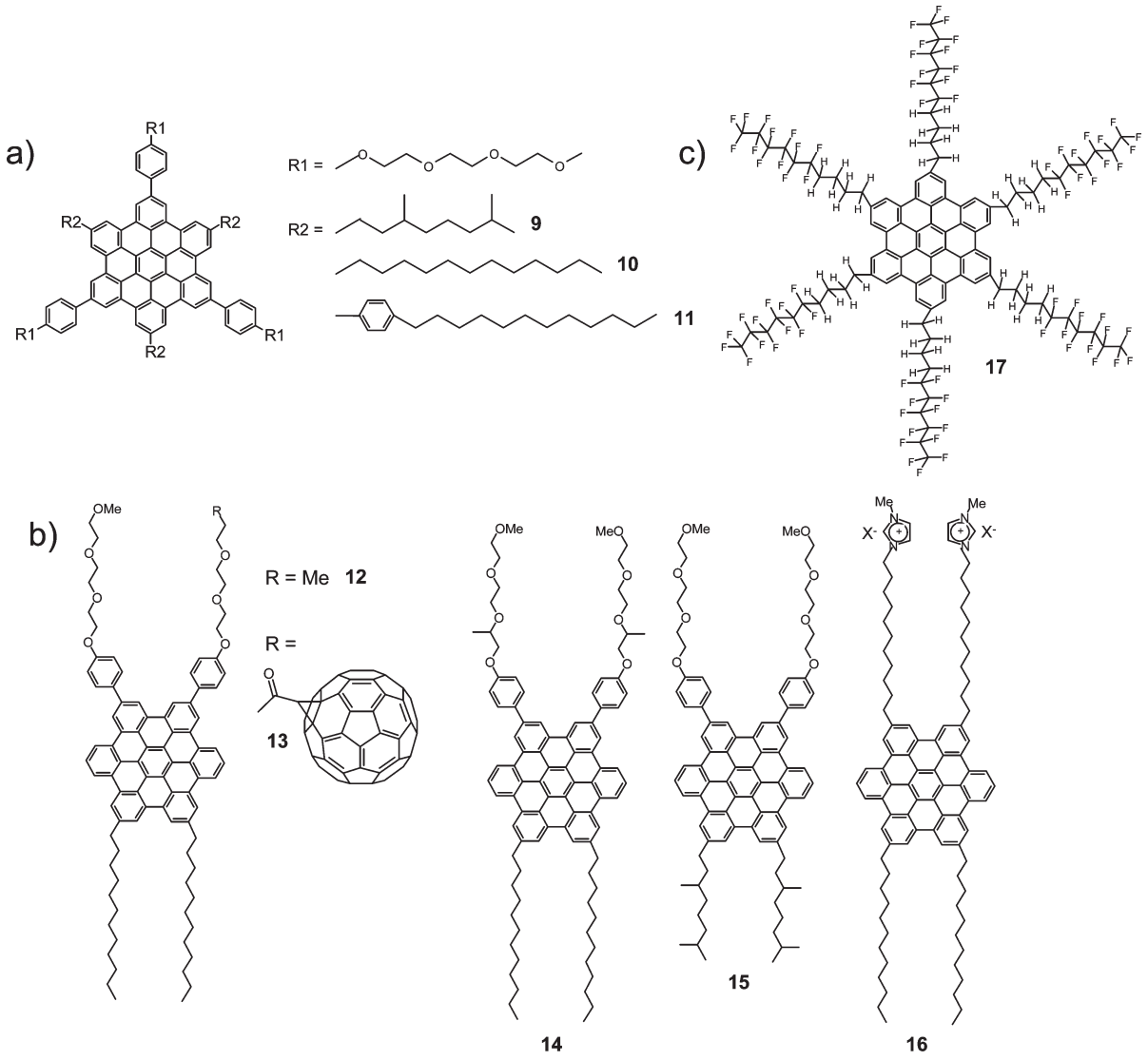

Figure 8. HBCs organize into nanotubes and nanofibers because of peripheral phase separation of the side chains: amphiphilic HBCs with (a) alternating chain arrangement and (b) gemini-shape, and (c) perfluoroalkylated HBC.

objects are based on individual columns well oriented along the fiber direction (Figure 7d). In the case of **8**, the supramolecular order is related to the methoxy units at the meta positions.

Another approach to control the nanostructures comprises amphiphilic PAHs with hydrophilic−hydrophobic interactions in the core periphery (Figure 8). The distribution of the substitutions of different type around the molecule plays a crucial role for the self-assembly. Hydrophobic and hydrophilic side chains are attached in an alternating fashion at the compounds **9**−**11**, whereby the thermotropic properties, aggregation in solution, and morphology on the surface are manipulated by the steric demand of the hydrophobic alkyls.[54] During solution processing, linear chains (**10**) lead to long helical bundles in which the columns were aligned along these structures (Figure 9a,b), whereas only small globular droplets composed of randomly deposited material are formed for HBCs with bulky branched substituents (**9**).

Aida and co-workers have designed gemini-shaped (refers to dimeric amphiphile consisting of two amphiphilic moieties covalently linked by a spacer group) amphiphilic HBCs carrying two hydrophobic dodecyl and two hydrophilic triethylene glycol (TEG) chains on opposite disk sides (**12**−**15**).[55,56] In polar solvents, the molecules organize into several tens of micrometer long nanotubes consisting of helically rolled-up bilayer tapes (Figure 10) because of the incompatibility of the side chains. In contrast to the alternating substituted HBCs **9**−**11**, in the case of **12**−**15**, the π-stacking direction is perpendicular to the tube axis. The single helical sense of these nanotubes is determined by the chiral centers in the hydrophilic fraction (**14**).[57] These nanotubes were also observed for HBCs with large hydrophobic groups, such as norbornene,[58] and trinitrofluorenone[59] pendants at the termini of the ethylene glycol chains. However, identical to the alternating decorated HBCs, no nanotube growth occurrs for **15** because high steric demand of the branched alkyls.[60] Despite the introduction of a bulkly fullenere derivative, compound **13** with a covalently linked C60 pendant self-organize into a coaxial nanotube whose wall consists of a stacked HBC array, whereas the nanotube surface is fully covered by a molecular layer of clustering

C60 (see illustration in Figure 10).[61] An ambipolar charge transport in a FET and a photovoltaic response upon light illumination are measured for such coaxial donor−acceptor heterojunction configuration. Electrodeless flashphotolysis time-resolved microwave conductivity technique reveal intratubular hole mobility of 2.0 $cm^2/(V\ s)$.

When the triethylene glycol chains are replaced by imidazolium ion pendants (**16**) for these gemini-shaped amphiphilic HBCs, filled fibers are obtained: These fibers revealed strong size and shape sensitivity to the solvent evaporation rate.[62] The mechanism of the fiber growth is related to the combination of π-stacking between the aromatic cores and ion−ion interactions of the imidazolium salts.

The above-described nanostructures are based mainly on the local phase separation of hydrophobic and hydrophilic side chains attached in different fashions at the aromatic core. Peripheral phase separation as a driving force for self-organization of PAHs can also occur along individual substituents which consist of a perfluoroalkylated and an alkylated section. Deposited from fluorocarbon-based solvent these HBC molecules (**17**) (Figure 8c) assemble into long monostranded molecular stacks.[63,64] Thereby, the flexible alkylated moieties play a key role during the fiber formation and act as a spacer between the rigid aromatic core and the semirigid perfluorinated tail.

The development of high-performance silicon-based integrated circuits technology over the last decades is mainly based on a remarkable down-scaling process that will encounter in the near future critical barriers and even fundamental physical limitations to any further size reduction. New molecular electronics, in which the electrode gap is bridged by single molecules or carbon nanotubes, can maybe overcome the challenge in miniaturization.[65,66] Nanotubes and nanofibers assembled by single PAH molecules enable a broad chemical modification of these nanostructures and their further applications, e.g., in sensors. Sensors based on quasi-2D random networks of carbon nanotubes and organic molecules can be used in medical areas to detect lung cancer from the breath.[67] The sensor consists of a two-terminal chemiresistor with a thin quasi 2D random network of intersecting carbon nanotubes which create multiple conductive paths between two interdigitated electrodes (illustration in Figure 11). Functionalization of the carbon nanotubes by a spongelike overlayer of alkylated HBCs improves the diagnostic sensor accuracy and selectivity for specific volatile organic compounds which can be typically found in exhaled breath of persons with lung cancer. The increase in sensitivity is attributed to a swelling of the HBC film during exposure to the nonpolar volatile compounds creating scattering centers in the underlying nanotubes.[68] The sensitivity to nonpolar and polar analytes depends on the degree of HBC coverage due to morphology changes in

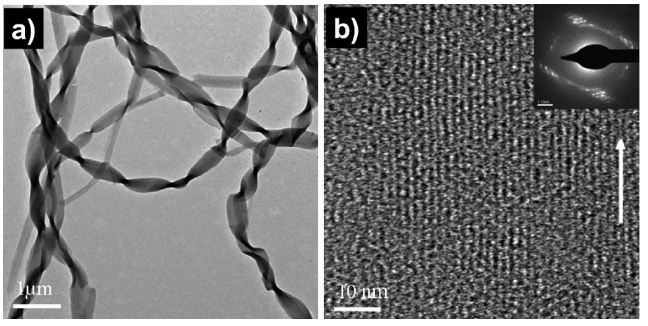

Figure 9. (a) Electron microscopy of **10**, the nanostructures were grown from MeOH:$CHCl_3$ = 2:1 solution, (b) HRTEM image displaying columnar structures of **10** within such fiber (inset: electron diffraction pattern with reflections assigned to the π-stacking distance of 0.35 nm). Adapted with permission from ref[54]. Copyright 2009 American Chemical Society.

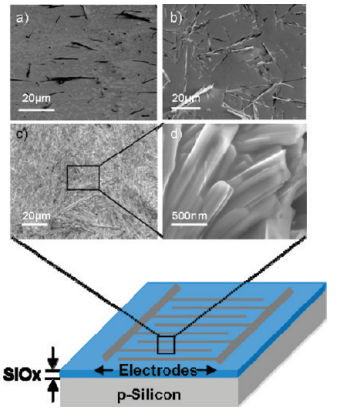

Figure 11. Schematic illustration of a chemiresistor and scanning electron images of random networks of carbon nanotubes with (a) 10, (b) 30, and (c, d) 90% of **4** film coverage. Adapted with permission from ref[69]. Copyright 2010 Wiley-VCH Verlag GmbH & Co. KGaA.

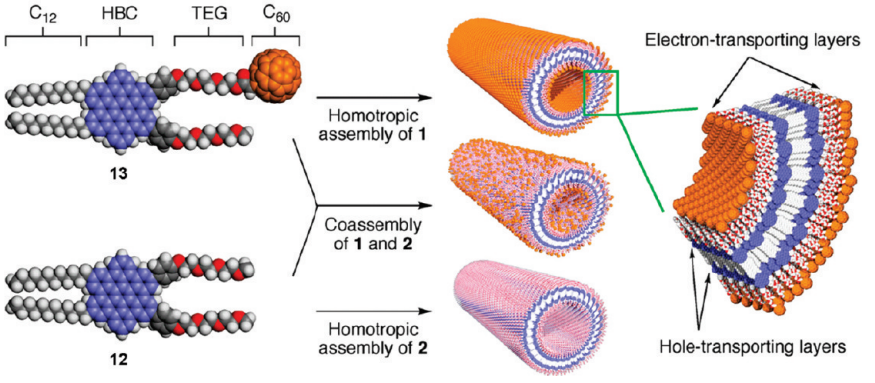

Figure 10. Hierarchical structure formation of a nanotube consisting of gemini-shaped **12** and **13**. Schematic illustration of the wall structure of the nanotube of **13** with the electron-transporting molecular layer of clustering C60 (orange) and a hole-transporting layer of HBC units (blue). Reprinted with permission from ref[61]. Copyright 2009 National Academy of Sciences, USA.

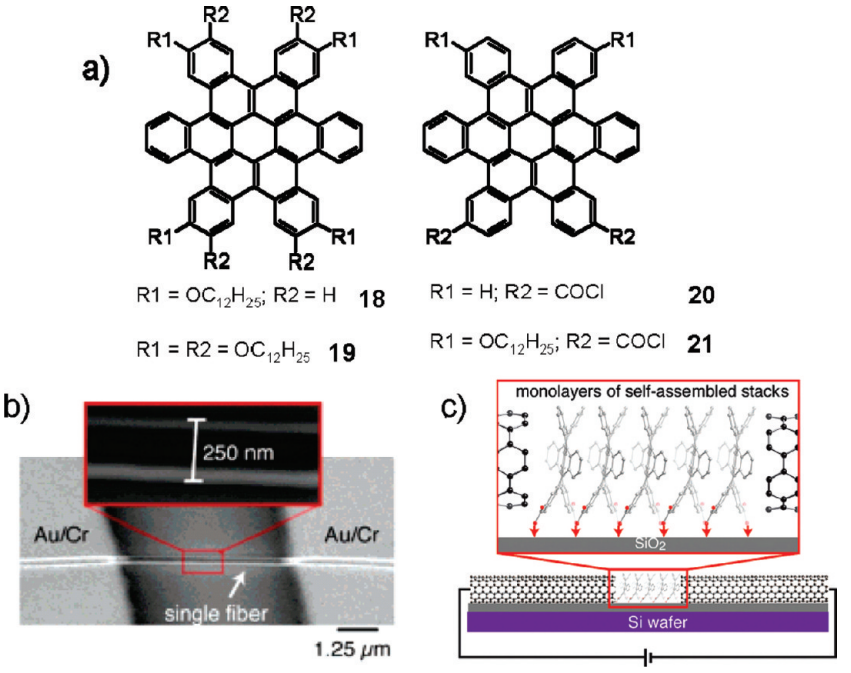

Figure 12. (a) Hexa-*cata*-hexabenzocoronene derivatives. Nanodevices based on PAHs: (b) image of an isolated fiber of **19** that spans electrodes in a FET device, (c) setup of a molecular sensor based on monolayers of **20** or **21** with groups capable to form covalent bondings to the silicon oxide surface. Reprinted with permission from ref [75]. Copyright 2006 National Academy of Sciences, U.S.A.

the bilayer structure (Figure 11).[69] This may allow the development of a cost-effective, portable, and noninvasive diagnostic tool.

The application of individual nanoscale fibers in FETs for miniaturization requires adequate handling techniques to manipulate and contact these nanoobjects. The procedures are well-developed for inorganic nanofibers and carbon nanotubes and can be also applied to self-assembled organic semiconductors.[70] For instance, the pick-and-place method is based on the utilization of an elastomer stamp which is pressed into a mat of single fibers.[71] In this way, a few wires are transferred to the stamp that is subsequently pressed onto the device substrate for deposition so that the objects span the electrodes. This procedure is successfully applied for nanostacks of **19** which are exploited in FET devices (Figure 12a).[71] In a top contact configuration, a charge-carrier mobility of holes of 0.02 $cm^2/(V\,s)$ is observed and takes place along the columnar stacks of **19**, which are oriented in the fiber axis. This mobility value is in the same range as obtained for spin-coated 4-fold alkoxy substituted liquid crystalline **18**.[72] The configuration of **18** can be separated into two π-systems. The inner radialene core leads to a one-dimensional charge transport, whereas the outer out-of-plane alkoxyphenyl rings insulate the inner pathway.[73] The charge-carrier mobility of **18** is increased up to 0.1 $cm^2/(V\,s)$ for a bilayer structure with an array of carbon nanotubes as an underlayer and **18** as overcoat.[74] This significant improvement in mobility is attributed to the modulation by the carbon nanotube density.

In molecular sensors, a molecule interacts with an analyte to produce a detectable change. This can also occur in a modified field-effect transistor in which the current changes due to molecular interactions between the organic semiconductor and analyte. Compounds **20** and **21** are covalently bonded as a monolayer to a silicon oxide surface of a transistor silicon wafer. As source and drain electrodes, individual metallic single-walled carbon nanotubes are used that are separated through an oxidative cutting by only a few nanometers from each other (Figure 12b).[75] In the short transistor channel, the molecules are arranged laterally into columns, while the device characteristics vary during exposure to electron-deficient molecules. This controlled reversible variation in current under different conditions confirms the successful operation as sensor.

The above-described fibers are formed by self-assembly of solution processed building blocks. The fiber shape and structure depend on the molecular interactions and the processing conditions. Hereby, templating is an alternative approach to control the fiber geometry and the molecular arrangement and orientation within the nanoobjects. Microporous inorganic membranes with a well-defined pore diameter are used as templates which can provide nanoscopic one-dimensional fibers or tubes after the pores are filled with the organic material either from the isotropic melt or solution.[76] In subsequent steps, the molecules are transferred into solid-state and the inorganic template is removed, yielding tubular or filled nanofibers with regular shape adjusted by the geometric confinement of the pores (Figure 13a).[77]

For instance, after filling the pores of an aluminum oxide template with discotic **5** from the isotropic melt and subsequent crystallization, the molecules self-align into highly ordered structures.[78] The structural analysis indicates an edge-on molecular orientation at the pore walls and an alignment of the columnar stacks along the pores. An identical organization in such templates is observed for melt processed discotic triphenylenes.[79,80] The aluminum oxide membrane is carefully dissolved and intact filled fibers are

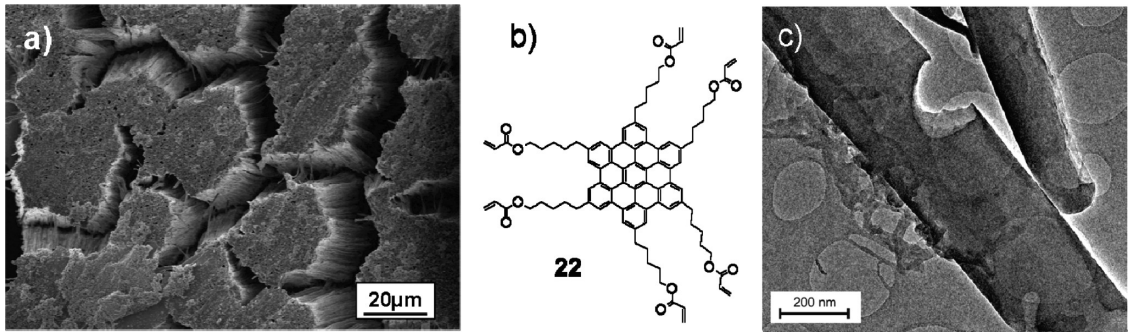

Figure 13. (a) Nanofibers obtained from **5** by melting processing, (b) HBCs equipped with functional acrylate groups (**22**) for cross-linking and c) nanotubes of cross-linked **22** as obtained from solution deposition into the membrane pores. Reprinted with permission from ref [81]. Copyright 2010 Wiley-VCH Verlag GmbH & Co. KGaA.

attained. As expected, the same molecular organization occurs in the fibers as before in the pores (Figure 13a). In all cases, the melt processing of PAHs results in filled wires. To obtain hollow tubes, HBCs equipped with functional acrylate groups (**22**) for thermal cross-linking (Figure 13b) are solution deposited into the pores.[81] When the inorganic template is removed, well-defined mechanical stable, nano-objects are found. Electron diffraction indicates that columnar structures are oriented along the tube axis (Figure 13c). It is interesting to note that processing the HBCs **5** and **22** from different states of matter, melt and solution, into the pores results for both cases in a unixial orientation of the stacks along the nano-objects. It is assumed that this alignment is formed already in the membrane because of a temperature/concentration gradient established along the pores during cooling the melt or solvent evaporation. Such prealignment in the template can be explored in pyrolysis leading to graphite nanotubes in which the graphitic sheets are perpendicular to the tube wall.[82] This arrangement is different from conventional carbon nanotubes, in which the graphene layer is directed along the tube axis.

5. Continuous Thin Layers for Transistors and Solar Cells

The previous section described the growth and application of single fibrous structures in miniaturized electronic devices. Hereby, the focus is on the growth control of the nanoobjects and their adequate transfer and implementation in the device. In bulk device structures, orientation and morphology play major roles on the performance which is a direct function of the defect density in the active layer. Structural disorder and pronounced grain boundaries act as charge carrier traps and limit the device operation.[83,84] As mentioned before, the intrinsic charge carrier mobilities of alkylated PAHs determined for the local scale are few orders of magnitude higher in comparison to FET mobility. A defect-free arrangement of the columnar one-dimensional pathways can maximize the charge migration between the source and drain electrodes. Furthermore, the stacks need to be aligned in the direction of the charge carrier transport, which takes place parallel to the surface, while the disk-shaped PAHs are edge-on organized on the FET substrate. For efficient solar cell applications, it is assumed that a molecular face-on and a subsequent homeotropic alignment promote the charge transport vertical to the surface between the top and bottom electrodes. The correlation between the columnar orientation of the molecules on the surface and the direction of the charge transport is apparent in time-of-flight (TOF) measurements (Figure 14). In this example, compounds **3** and **5**, which arrange in an opposite fashion on the surface, are filled from the melt into a sandwich electrode geometry. During the TOF experiment, the charge carrier drift perpendicular to the surface is monitored and the mobility and transport character are determined. A structural study by synchrotron radiation microfocused X-ray scattering indicated an edge-on arrangement of **5** in spherulitic domains (Figure 14c) in which the stacks are radially oriented from the nucleation center.[85] For this sample, no TOF signal could be detected because the long branched alkyl substituents blocked a charge carrier transport perpendicular to the columnar pathway (Figure 14e).[86] The formation of a homeotropic phase has been reported for various discotic systems, however, the mechanism behind this is not fully understood.[87−90] A dispersive transport mechanism was observed for **3**, when the thin film is cooled too quickly and disordered domains with grain boundaries and columnar defects as scattering sites for charges are created. A distinct nondispersive hole transport with a pronounced plateau in the signal is observed for slowly processed and macroscopically highly ordered monodomains (Figure 14b). This characteristic behavior is attributed to an undisturbed pathway for the charges carriers (Figure 14d).

To obtain thin layers of PAHs with an adequate orientation and order for FET applications, the molecules have to be processed by suitable methods. The next paragraphs give a brief summary over the most efficient alignment technologies utilized for discotic PAHs and their successful implementation in transistors. All methods are based on solution processing, which is most attractive for up-scaling in industrial manufacturing.

Zone casting is especially interesting for potential commercialization since it is a continuous procedure. During the operation, a nozzle deposits a solution, which is permanently supplied, onto a moving substrate and a meniscus is formed between the nozzle and the substrate (Figure 15a). When the solvent evaporates a concentration gradient is established, which is the driving force for the structure growth. Finally, at the critical concentration the material

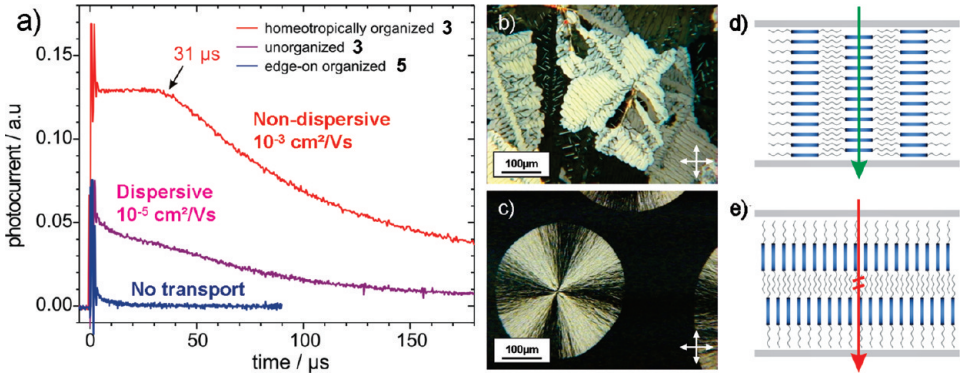

Figure 14. (a) Time-of-flight hole current transients of **3** and **5** oriented differently toward the surface, polarized microscopy images of (b) **3** and (c) **5**, schematic illustration of homeotropic **3** and edge-on **5** (arrows indicate the charge-carrier transport through the layer). Reprinted with permission from ref [86]. Copyright 2006 Wiley-VCH Verlag GmbH & Co. KGaA.

nucleates on substrate surface as an oriented film. A broad range of organic systems including organic semiconductors and polymers can be processed by this technique.[91−93]

Crystalline and liquid crystalline PAHs of different size and shape were macroscopically oriented by zone casting.[94] Especially pronounced solution aggregation and preaggregation of the molecules are essential factors for the zone casting alignment. For instance, **4** was processed into highly ordered thin films in which the columnar structures were uniaxially oriented in the deposition direction.[95] In the macroscopic "single-crystalline" surface layers, the HBC discs arranged in an edge-on manner.[96,97] Interestingly, it was possible to reversibly switch the thin film from nonbirefringence to birefringence in polarized light by changing the phase from crystalline to liquid crystalline.[98,99] This effect was attributed to the molecular reorganization from herringbone to nontilted packing at the phase transition. Although unoriented drop-cast films of **4** showed isotropic mobilities up to 1×10^{-4} cm^2/(V s),[100] the incorporation of the zone cast layers into a top contact FET resulted in improved performance with 1×10^{-2} cm^2/(V s) and good on−off ratio of 1×10^4. Furthermore, a mobility anisotropy along and perpendicular to the columnar pathways was determined confirming the one-dimensional character for this kind of organic semiconductor.

Exposed in an external magnetic field, most aromatic molecules orient with their ring plane along the gradient.[101,102] This principle has been exploited for the macroscopic alignment of alkylated PAHs (Figure 15b). Compound **23** was deposited from solution onto a transistor in the presence of a 20 T magnetic field.[103] A strong effect on the organization and morphology was observed. The discs were edge-on arranged with their planes along the applied magnetic field, whereas columns were directed by 40° to the applied gradient. The film topography revealed individual fibers aligned perpendicular to the magnetic field direction (Figure 16). A strong anisotropy was also determined for the FET performance. Charge carrier mobilities up to 6×10^{-4} cm^2/(V s) were measured perpendicular direction to the magnetic field and only 6×10^{-6} cm^2/(V s) (Figure 16) parallel.

An identical FET mobility of 5×10^{-4} cm^2/(V s) along the columnar alignment has been reported for films of

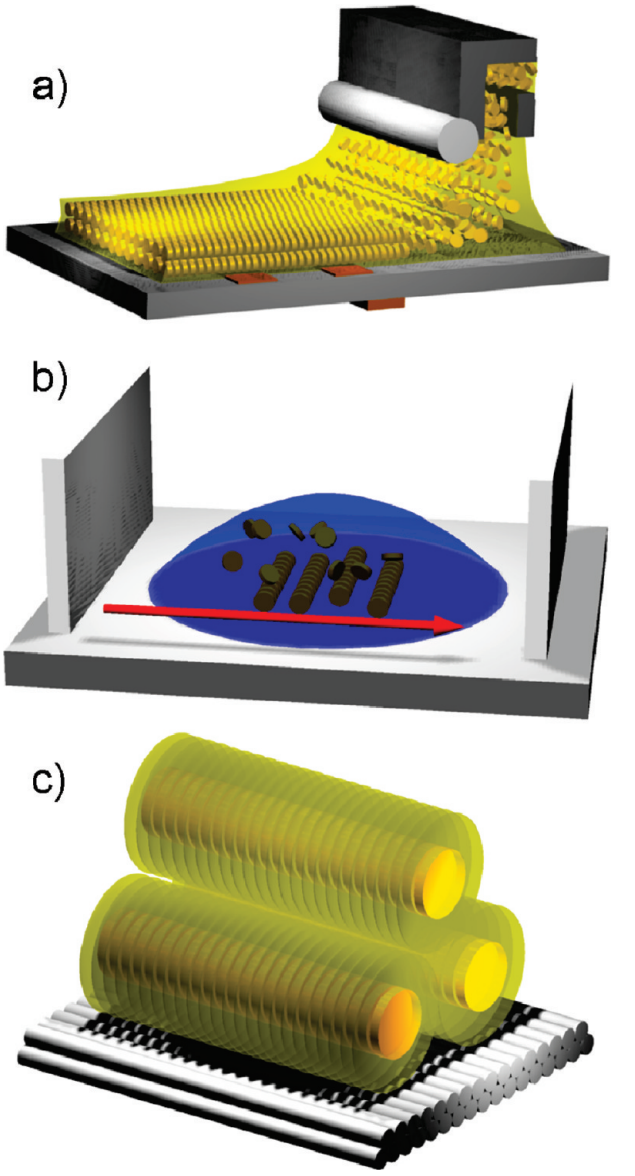

Figure 15. Schematic illustrations of different solution alignment techniques of HBCs for the application in FETs: (a) zone-casting, (b) in magnetic field, and (c) prealigned PTFE layer.

23 oriented on preoriented and friction-deposited poly(tetrafluoroethylene) (PTFE) (Figure 15c).[104] Thereby,

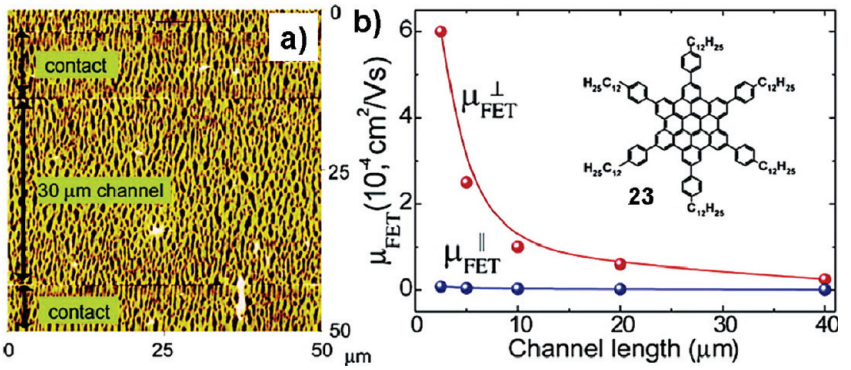

Figure 16. (a) Atomic force microscopy (AFM) image of magnetically aligned **23**-based FET and (b) dependence of the mobility on the channel length for perpendicular and parallel current directions to the magnetic field. Adapted with permission from ref [103]. Copyright 2005 American Chemical Society.

the solution deposited molecules grow in an epitaxial fashion on the PTFE surface yielding a macroscopic orientation. The columnar stacks are arranged parallel to the underlying PTFE chains. Furthermore, the intercolumnar 2D unit cell is closely related to the underlaying PTFE layer.[105−107]

In contrast to FETs, the performance of organic solar cells depends on a broad parameter set. The most efficient device structure is based on heterojunction mixtures of two blended compounds with dissimilar electronic affinity.[108,109] The active layers are solution processed by spin-coating both the donor and acceptor components during which the compounds phase separate to establish the heterojunction structure. Thereby, the molecular orientation in the domains is not well controlled. The phase separation is influenced by the solvent, concentration and rotation speed. Spin-coating of **23** as the donor and perylene diimide (PDI) as the acceptor a vertical phase separation arises between the compounds in the thin film, which leads to a large surface contact and finally to a high external quantum efficiency of 34% at 490 nm (Figure 17a).[110]

A systematic study on a series of HBCs carrying side chains of different length (**3**, **4**, and **5**) revealed that the HBC chromophore is diluted and absorbs less light when long substitutions are attached.[111] Furthermore, compounds with short alkyls show high crystallinity, which in turn improves the interfacial donor/acceptor separation and promotes the charge separation. Long side chains ensure the solubility and thus the processability, but lead to two major disadvantages. First, donor−acceptor molecules do not phase separate well and pack within the same columnar stacks limiting the charge transport.[112] Second, long insulating side chains around the aromatic conducting fraction decrease the exciton polarization and separation in the photovoltaic cell. On the other hand, long branched chains can induce liquid crystallinity and can allow self-healing of structural defects at elevated temperatures as in the case of $D_{3\ h}$ symmetric triangle shaped PAHs (**24**−**25**, Figure 17b).[16] The order and intracolumnar packing of compound **25** significantly improved after annealing and increased the solar cell efficiency. A normalized external quantum efficiency value was determined by taking into consideration the ratio between the aromatic chromophore

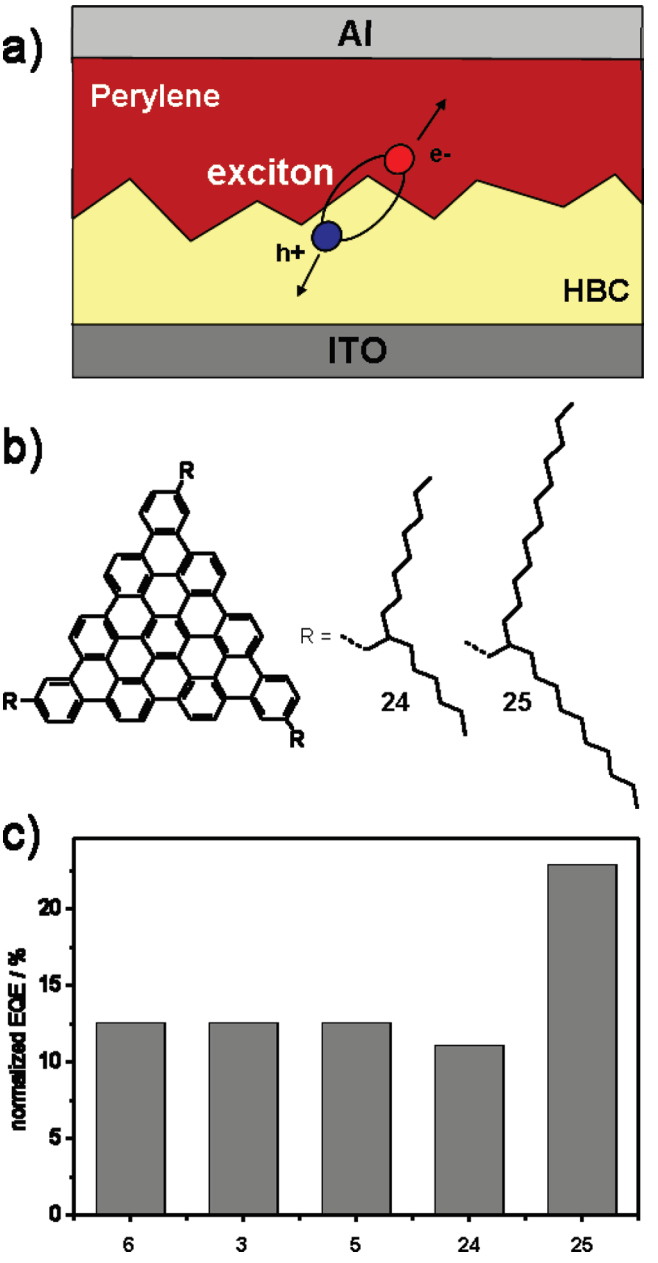

Figure 17. (a) Schematic illustration of a heterojunction structure with phase separation between vertical layers of the acceptor perylene and donor HBC, (b) triangle-shaped PAHs for photovoltaics, normalized external quantum efficiency for differently substituted PAHs.

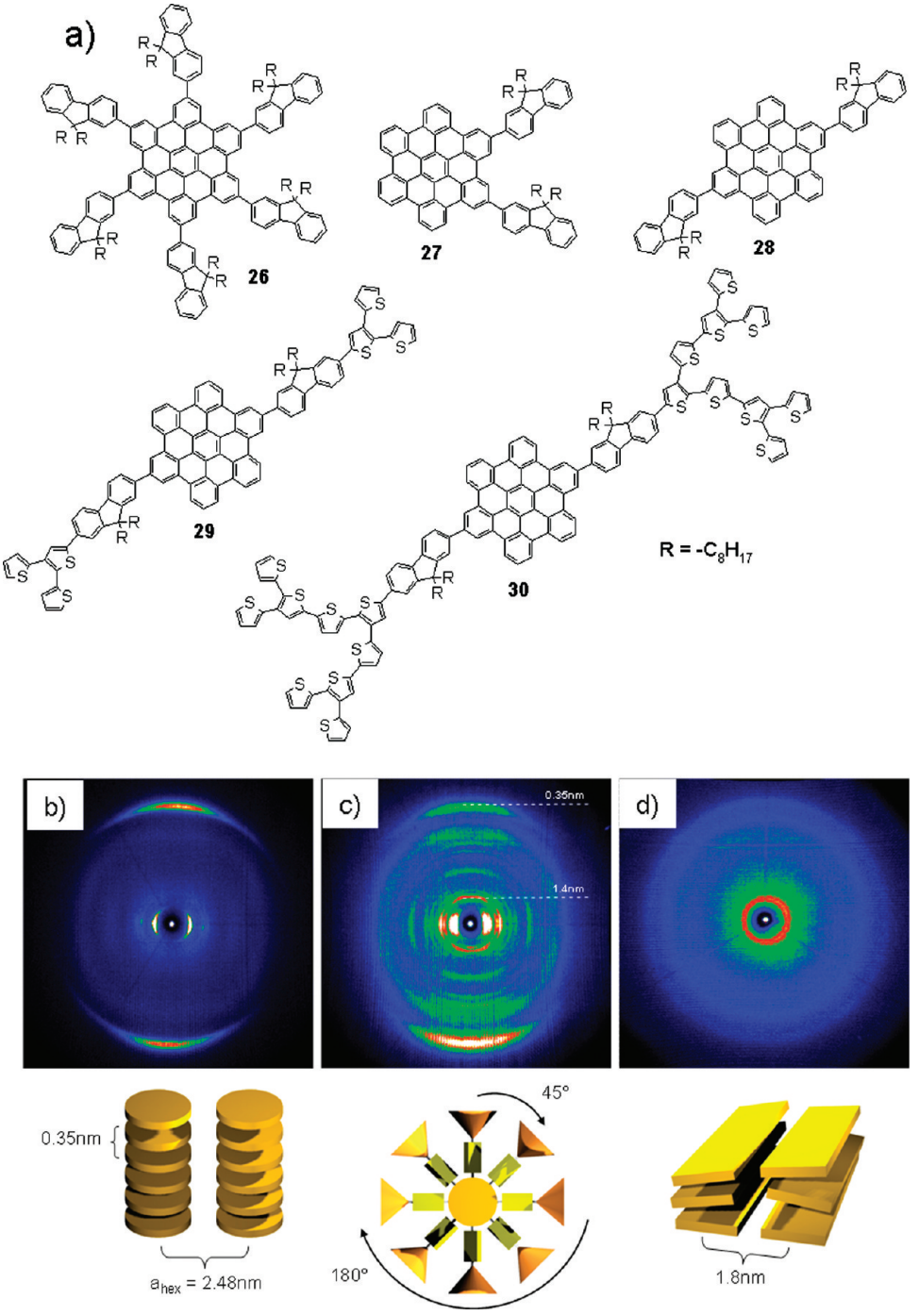

Figure 18. (a) 9,9-dioctylfluorenyl substituted HBCs without and with thiophene dendrons for solar cell application and 2D-WAXS patterns of (b) **26**, (c) **27**, and (d) **28** with their corresponding molecular packing. Adapted with permission from ref [116]. Copyright 2010 American Chemical Society.

and the insulating alkyl fraction (Figure 17c). The comparison between different discotic PAHs revealed the highest value for **25**.

Because of the insulation of the inner aromatic stack by the peripheral alkyl chains an alternative concept has been developed. Thereby, the HBC disk is substituted by conjugated substituents which in turn carry the solubilizing group (Figure 18).[113] The incorporation of a 9,9-dioctylfluorenyl moiety not only ensures excellent solubility and the potential for further derivatization, but strongly affects the intermolecular interactions. Hexasubstituted HBC (**26**) revealed only weak interaction in solution and poor solid- state order due to the high steric hindrance of the attached fluorene groups, whereas bis-substituted compounds (**27** and **28**) showed pronounced self-assembly properties (Figure 18a).[114] The degree of order of the bulk structure played an essential role for the solar cell and FET performance. Energy level data of the three HBCs indicated [6,6]-phenyl-C61-butyric acid methyl ester (PC61BM) as the suitable acceptor candidate for active layer blends in bulk heterojunction solar cells. Low device performance was observed for the poorly ordered **26**, whereas **27** and **28** yielded improved device characteristics. For instance, a field-effect mobility of 2.8×10^{-3} $cm^2/(V\ s)$

and a power conversion efficiency of 1.5% were achieved for spin-cast **28**.

On the basis of the successful implementation of the fluorene functionalized HBCs in solar cells, this molecular design has been extended. The sunlight harvesting was improved by broadening the absorption profile of the organic materials and the conversion of the light energy absorbed into electric current became more efficient. As a new molecular element, thiophenes were introduced because these compounds have emerged as one of the most important classes of materials in the area of organic electronics over the past decade (Figure 18a).[115] The already described fluorenyl HBC **28** was applied as the scaffold for molecular organization, whereas a series of thiophene dendrons were attached in the periphery.[116] Columnar suprastructures were found for **28** and **29** (Figure 18b,c). In contrast, **30** functionalized with the most bulky dendrons revealed poor order (Figure 18d), but also a broadened UV−vis absorption profile. This characteristic light absorption resulted in high power conversion efficiency of 2.5% for **30**.

6. Conclusions

During the past decade, there has been an enormous progress in the field of organic electronics employing PAHs. The understanding of correlation between their physical properties and the device applications has been improved significantly.

In general, a broad range of parameters can influence the solar cell efficiency of liquid crystalline PAHs. Although the order and the orientation of molecules on the surface are not optimized, the fluorene functionalized HBC-based chromophors reveal good efficiencies in comparison to other solution processed, conjugated small molecules. The high device performance is mainly obtained because of a light harvesting over a broad range of wavelengths. Therefore, it can be expected that close packing and homeotropic alignment of the donor molecules will further boost the efficiencies. First reports for homeotropically oriented discotic donor−acceptor mixtures indicate this trend.[117,32] Self-healing through annealing in the liquid crystalline state at elevated temperatures tightens the molecular packing and promotes the solar cell operation.

However, the role of thermal treatment in the liquid-crystalline phase improving the performance is not observed for FETs. Annealing at higher temperatures even lowers the charge carrier mobilities due to disorder of the first semiconducting PAH monolayer on the surface. On the other hand, it has been well proven that the processing of highly long-range ordered films improves the migration of carriers between the electrodes. But the mobilities are still by far lower in comparison to the intrinsic values for PAHs. This discrepancy is related to the fact that only one single defect over few micrometers is sufficient to disrupt the transport through the columnar pathway. There are two alternatives that can solve this problem. For the first one, recent literature[118] suggests that covalent grafting of liquid crystalline PAHs on the surface through an anchor-group reduces the π-stacking distance below the values observed in the bulk, and enhances the ordering in the thin accumulation layer of the FET considerably. In second approach, the dimensionality of charge transport can be increased from one- to two-dimension by adjustment of the molecular design. An appropriate molecular structure can include conjugated bridges between the columnar stacks which favor an intercolumnar motion of charges and, via this bypass, help to overcome the influence of local structural defects on the charge transport.

Acknowledgment. The German Science Foundation (Korean-German IR TG), the European Community's Seventh Framework Programme ONE-P (grant agreement 212311), DFG Priority Program SPP 1355, DFG MU 334/32-1, DFG Priority Program SPP 1459, and ESF Project GOSPEL (ref 09-EuroGRAPHENE-FP-001).

References

(1) Tang, C. W. *Appl. Phys. Lett.* **1986**, *48*, 183.
(2) Burroughes, J. H.; Jones, C. A.; Friend, R. H. *Nature* **1988**, *335*, 137.
(3) Tsumura, A.; Koezuka, H.; Ando, T. *Appl. Phys. Lett.* **1986**, *49*, 1210.
(4) Forrest, S. R. *Nature* **2004**, *428*, 911.
(5) Arias, A. C.; MacKenzie, J. D.; McCulloch, I.; Rivnay, J.; Salleo, A. *Chem. Rev.* **2010**, *110*, 3.
(6) Blom, P. W. M.; Mihailetchi, V. D.; Koster, L. J. A.; Markov, D. E. *Adv. Mater.* **2007**, *19*, 1551.
(7) Allard, S.; Forster, M.; Souharce, B.; Thiem, H.; Scherf, U. *Angew. Chem., Int. Ed.* **2008**, *47*, 4070.
(8) Tsao, H. N.; Müllen, K. *Chem. Soc. Rev.* **2010**, *39*, 2372.
(9) Park, Y. D.; Lim, J. A.; Lee, H. S.; Cho, K. *Mater. Today* **2007**, *10*, 46.
(10) Sergeyev, S.; Pisula, W.; Geerts, Y. H. *Chem. Soc. Rev.* **2007**, *36*, 1902.
(11) Laschat, S.; Baro, A.; Steinke, N.; Giesselmann, F.; Hägele, C.; Scalia, G.; Judele, R.; Kapatsina, E.; Sauer, S.; Schreivogel, A.; Tosoni, M. *Angew. Chem., Int. Ed.* **2007**, *46*, 4832.
(12) Pisula, W.; Zorn, M.; Chang, J. Y.; Müllen, K.; Zentel, R. *Macromol. Rapid Commun.* **2009**, *30*, 1179.
(13) Wu, J.; Pisula, W.; Müllen, K. *Chem. Rev.* **2007**, *107*, 718.
(14) Watson, M. D.; Fechtenkötter, A.; Müllen, K. *Chem. Rev.* **2001**, *101*, 1267.
(15) Simpson, C. D.; Brand, J. D.; Berresheim, A. J.; Przybilla, L.; Räder, H. J.; Müllen, K. *Chem.—Eur. J.* **2002**, *8*, 1424.
(16) Feng, X.; Liu, M.; Pisula, W.; Takase, M.; Li, J.; Müllen, K. *Adv. Mater.* **2008**, *20*, 2684.
(17) Böhme, T.; Simpson, C. D.; Müllen, K.; Rabe, J. P. *Chem.—Eur. J.* **2007**, *13*, 7349.
(18) Tomovic, Z.; Watson, M. D.; Müllen, K. *Angew. Chem., Int. Ed.* **2004**, *43*, 755.
(19) van de Craats, A. M.; Warman, J. M.; Fechtenkötter, A.; Brand, J. D.; Harbison, M. A.; Müllen, K. *Adv. Mater.* **1999**, *11*, 1469.
(20) Pisula, W.; Tomovic, Z.; Simpson, C.; Kastler, M.; Pakula, T.; Müllen, K. *Chem. Mater.* **2005**, *17*, 4296.
(21) Fontes, E.; Heiney, P. A.; Dejeu, W. H. *Phys. Rev. Lett.* **1988**, *61*, 1202.
(22) Wu, J.; Fechtenkötter, A.; Gauss, J.; Watson, M. D.; Kastler, M.; Fechtenkötter, C.; Wagner, M.; Müllen, K. *J. Am. Chem. Soc.* **2004**, *126*, 11311.
(23) Wasserfallen, D.; Fischbach, I.; Tchebotareva, N.; Kastler, M.; Pisula, W.; Jäckel, F.; Watson, M. D.; Schnell, I.; Rabe, J. P.; Spiess, H. W.; Müllen, K. *Adv. Funct. Mater.* **2005**, *15*, 1585.
(24) Dou, X.; Pisula, W.; Wu, J.; Bodwell, G. J.; Müllen, K. *Chem.—Eur. J.* **2008**, *14*, 240.
(25) Feng, X.; Pisula, W.; Zhi, L.; Takase, M.; Müllen, K. *Angew. Chem., Int. Ed.* **2008**, *47*, 1703.
(26) Feng, X.; Pisula, W.; Takase, M.; Dou, X.; Enkelmann, V.; Wagner, M.; Ding, N.; Müllen, K. *Chem. Mater.* **2008**, *20*, 2872.
(27) Fischbach, I.; Pakula, T.; Minkin, P.; Fechtenkötter, A.; Müllen, K.; Spiess, H. W.; Saalwachter, K. *J. Phys. Chem. B* **2002**, *106*, 6408.
(28) Fischbach, I.; Ebert, F.; Spiess, H. W.; Schnell, I. *Chem. Phys.Chem.* **2004**, *5*, 895.
(29) Boden, N.; Bushby, R. J.; Clements, J.; Movaghar, B.; Donovan, K. J.; Kreouzis, T. *Phys. Rev. B* **1995**, *52*, 13274.
(30) Lever, L. J.; Kelsall, R. W.; Bushby, R. J. *Phys. Rev. B* **2005**, *72*, 035130.
(31) Warman, J. M.; van de Craats, A. M. *Mol. Cryst. Liq. Cryst.* **2003**, *396*, 41.
(32) Käfer, D.; Bashir, A.; Dou, X.; Witte, G.; Müllen, K.; Wöll, C. *Adv. Mater.* **2010**, *22*, 384.
(33) Boden, N.; Bushby, R. J.; Clements, J. *J. Chem. Phys.* **1993**, *98*, 5920.
(34) Simmerer, J.; Glüsen, B.; Paulus, W.; Kettner, A.; Schuhmacher, P.; Adam, D.; Etzbach, K. H.; Siemensmeyer, K. J.; Wendorff, H.; Ringsdorf, H.; Haarer, D. *Adv. Mater.* **1996**, *8*, 815.

(35) Bushby, R. J.; Lozman, O. R. *Curr. Opin. Solid State Mater.* **2002**, *6*, 569.
(36) van de Craats, A. M.; Siebbeles, L. D. A.; Bleyl, I.; Haarer, D.; Berlin, Y. A.; Zharikov, A. A.; Warman, J. M. *J. Phys. Chem. B* **1998**, *102*, 9625.
(37) van de Craats, A. M.; Warman, J. M.; de Haas, M. P.; Adam, D.; Simmerer, J.; Haarer, D.; Schuhmacher, P. *Adv. Mater.* **1996**, *8*, 823.
(38) Prins, P.; Grozema, F. C.; Schins, J. M.; Patil, S.; Scherf, U.; Siebbeles, L. D. A. *Phys. Rev. Lett.* **2006**, *96*, 146601.
(39) van de Craats, A. M.; de Haas, M. P.; Warman, J. M. *Synth. Met.* **1997**, *86*, 2125.
(40) van de Craats, A. M.; Warman, J. M. *Adv. Mater.* **2001**, *13*, 130.
(41) Feng, X.; Marcon, V.; Pisula, W.; Hansen, M. R.; Kirkpatrick, J.; Grozema, F.; Andrienko, D.; Kremer, K.; Müllen, K. *Nat. Mater.* **2009**, *8*, 421.
(42) Feng, X.; Pisula, W.; Müllen, K. *J. Am. Chem. Soc.* **2007**, *129*, 14116.
(43) Feng, X.; Wu, J.; Ai, M.; Pisula, W.; Zhi, L.; Rabe, J. P.; Müllen, K. *Angew. Chem., Int. Ed.* **2007**, *46*, 3033.
(44) Pisula, W.; Tomovic, Z.; Watson, M. D.; Müllen, K.; Kussmann, J.; Ochsenfeld, C.; Metzroth, T.; Gauss, J. *J. Phys. Chem. B.* **2007**, *111*, 7481.
(45) Warman, J. M.; Piris, J.; Pisula, W.; Kastler, M.; Wasserfallen, D.; Müllen, K. *J. Am. Chem. Soc.* **2005**, *127*, 14257.
(46) Motoyanagi, J.; Yamamoto, Y.; Saeki, A.; Alam, Md. A.; Kimoto, A.; Kosaka, A.; Fukushima, T.; Seki, S.; Tagawa, S.; Aida, T. *Chem. Asian J.* **2009**, *4*, 876.
(47) Pisula, W.; Kastler, M.; Wasserfallen, D.; Mondeshki, M.; Piris, J.; Schnell, I.; Müllen, K. *Chem. Mater.* **2006**, *18*, 3634.
(48) Kirkpatrick, J.; Marcon, V.; Kremer, K.; Nelson, J.; Andrienko, D. *J. Chem. Phys.* **2008**, *129*, 094506.
(49) Kirkpatrick, J.; Marcon, V.; Nelson, J.; Kremer, K.; Andrienko, D. *Phys. Rev. Lett.* **2007**, *98*, 227402.
(50) Kastler, M.; Pisula, W.; Wasserfallen, D.; Pakula, T.; Müllen, K. *J. Am. Chem. Soc.* **2005**, *127*, 4286.
(51) Gao, P.; Beckmann, D.; Tsao, H. N.; Feng, X.; Enkelmann, V.; Baumgarten, M.; Pisula, W.; Müllen, K. *Adv. Mater.* **2009**, *21*, 209.
(52) Tsao, H. N.; Cho, D.; Andreasen, J. W.; Rouhanipour, A.; Breiby, D. W.; Pisula, W.; Müllen, K. *Adv. Mater.* **2008**, *21*, 209.
(53) Hoeben, F. J. M.; Jonkheijm, P.; Meijer, E. W.; Schenning, A. P. H. J. *Chem. Rev.* **2005**, *105*, 1491.
(54) Feng, X.; Pisula, W.; Kudernac, T.; Wu, D.; Zhi, L.; De Feyter, S.; Müllen, K. *J. Am. Chem. Soc.* **2009**, *131*, 4439.
(55) Hill, J. P.; Jin, W.; Kosaka, A.; Fukushima, T.; Ichihara, H.; Shimomura, T.; Ito, K.; Hashizume, T.; Ishii, N.; Aida, T. *Science* **2004**, *304*, 1481.
(56) Jin, W.; Yamamoto, Y.; Fukushima, T.; Ishii, N.; Kim, J.; Kato, K.; Takata, M.; Aida, T. *J. Am. Chem. Soc.* **2008**, *130*, 9434.
(57) Yamamoto, Y.; Fukushima, T.; Jin, W.; Kosaka, A.; Hara, T.; Nakamura, T.; Saeki, A.; Seki, S.; Tagawa, S.; Aida, T. *Adv. Mater.* **2006**, *18*, 1297.
(58) Yamamoto, T.; Fukushima, T.; Yamamoto, Y.; Kosaka, A.; Jin, W.; Ishii, N.; Aida, T. *J. Am. Chem. Soc.* **2006**, *128*, 14337.
(59) Yamamoto, Y.; Fukushima, T.; Suna, Y.; Ishii, N.; Saeki, A.; Seki, S.; Tagawa, S.; Taniguchi, M.; Kawai, T.; Aida, T. *Science* **2006**, *314*, 1761.
(60) Jin, W.; Fukushima, T.; Niki, M.; Kosaka, A.; Ishii, N.; Aida, T. *Proc. Natl. Acad. Sci. U.S.A.* **2005**, *102*, 10801.
(61) Yamamoto, Y.; Zhang, G.; Jin, W.; Fukushima, T.; Ishii, N.; Saeki, A.; Seki, S.; Tagawa, S.; Minari, T.; Tsukagoshi, K.; Aida, T. *Proc. Natl. Acad. Sci. U.S.A.* **2009**, *106*, 21051.
(62) El Hamaoui, B.; Zhi, L.; Pisula, W.; Kolb, U.; Wu, J.; Müllen, K. *Chem. Commun.* **2007**, *23*, 2384.
(63) Aebischer, O. F.; Aebischer, A.; Tondo, P.; Alameddine, B.; Dadras, M.; Güdel, H.-U.; Jenny, T. A. *Chem. Commun.* **2006**, 4221.
(64) Aebischer, O. F.; Aebischer, A.; Donnio, B.; Alameddine, B.; Dadras, M.; Güdel, H.-U.; Guillon, D.; Jenny, T. A. *J. Mater. Chem.* **2007**, *17*, 1262.
(65) Joachim, C.; Gimzewski, J. K.; Aviram, A. *Science* **2000**, *408*, 541.
(66) Avouris, P. *Acc. Chem. Res.* **2002**, *35*, 1026.
(67) Peng, G.; Trock, E.; Haick, H. *Nano Lett.* **2008**, *8*, 3631.
(68) Zilberman, Y.; Tisch, U.; Pisula, W.; Feng, X.; Müllen, K.; Haick, H. *Langmuir* **2009**, *25*, 5411.
(69) Zilberman, Y.; Tisch, U.; Shuster, G.; Pisula, W.; Feng, X.; Müllen, K.; Haick, H. *Adv. Mater.* **2010**, *22*, 4317.
(70) Huang, X. M. H.; Caldwell, R.; Huang, L.; Jun, S. C.; Huang, M.; Sfeir, M. Y.; O'Brien, S. P.; Hone, J. *Nano Lett.* **2005**, *5*, 1515.
(71) Xiao, S.; Tang, J.; Beetz, T.; Guo, X.; Tremblay, N.; Siegrist, T.; Zhu, Y.; Steigerwald, M.; Nuckolls, C. *J. Am. Chem. Soc.* **2006**, *128*, 10700.
(72) Xiao, S.; Myers, M.; Miao, Q.; Sanaur, S.; Pang, K.; Steigerwald, M. L.; Nuckolls, C. *Angew. Chem., Int. Ed.* **2005**, *44*, 7390.
(73) Cohen, Y. S.; Xiao, S.; Steigerwald, M. L.; Nuckolls, C.; Kagan, C. R. *Nano Lett.* **2006**, *6*, 2838.
(74) Harris, K. D.; Xiao, S.; Lee, C. Y.; Strano, M. S.; Nuckolls, C.; Blanchet, G. B. *J. Phys. Chem. C* **2007**, *111*, 17947.
(75) Guo, X.; Myers, M.; Xiao, S.; Lefenfeld, M.; Steiner, R.; Tulevski, G. S.; Tang, J.; Baumert, J.; Leibfarth, F.; Yardley, J. T.; Steigerwald, M. L.; Kim, P.; Nuckolls, C. *Proc. Natl. Acad. Sci. U.S.A.* **2006**, *103*, 11452.
(76) Steinhart, M.; Wendorff, J. H.; Greiner, A.; Wehrspohn, R. B.; Nielsch, K.; Schilling, J.; Choi, J.; Gösele, U. *Science* **2002**, *296*, 1997.
(77) Steinhart, M.; Wehrspohn, R. B.; Gösele, U.; Wendorff, J. H. *Angew. Chem., Int. Ed.* **2004**, *43*, 1334.
(78) Pisula, W.; Kastler, M.; Wasserfallen, D.; Davies, R. J.; Garcia-Gutierrez, M.-C.; Müllen, K. *J. Am. Chem. Soc.* **2006**, *128*, 14424.
(79) Steinhart, M.; Murano, S.; Schaper, A. K.; Ogawa, T.; Tsuji, M.; Gösele, U.; Weder, C.; Wendorff, J. H. *Adv. Funct. Mater.* **2005**, *15*, 1656.
(80) Steinhart, M.; Zimmermann, S.; Göring, P.; Schaper, A. K.; Gösele, U.; Weder, C.; Wendorff, J. H. *Nano Lett.* **2005**, *5*, 429.
(81) Kastler, M.; Pisula, W.; Davies, R. J.; Gorelik, T.; Kolb, U.; Müllen, K. *Small* **2007**, *3*, 1281.
(82) Zhi, L.; Wu, J.; Li, J.; Kolb, U.; Müllen, K. *Angew. Chem., Int. Ed.* **2005**, *44*, 2120.
(83) Salleo, A. *Mater. Today* **2007**, *10*, 38.
(84) Dimitrakopoulos, C. D.; Malenfant, P. R. L. *Adv. Mater.* **2002**, *14*, 99.
(85) Pisula, W.; Kastler, M.; Wasserfallen, D.; Pakula, T.; Müllen, K. *J. Am. Chem. Soc.* **2004**, *126*, 8074.
(86) Kastler, M.; Pisula, W.; Laquai, F.; Kumar, A.; Davis, R.; Baluschev, S.; Garcia-Gutierrez, M. C.; Wasserfallen, D.; Butt, H.-J.; Riekel, C.; Wegner, G.; Müllen, K. *Adv. Mater.* **2006**, *18*, 2255.
(87) De Cupere, V.; Tant, J.; Viville, P.; Lazzaroni, R.; Osikowicz, W.; Salaneck, W. R.; Geerts, Y. H. *Langmuir* **2006**, *22*, 7798.
(88) Grelet, E.; Bock, H. *Europhys. Lett.* **2006**, *73*, 712.
(89) Pisula, W.; Tomovic, Z.; El Hamaoui, B.; Watson, M. D.; Pakula, T.; Müllen, K. *Adv. Funct. Mater.* **2005**, *15*, 893.
(90) Wasserfallen, D.; Kastler, M.; Pisula, W.; Hofer, W. A.; Fogel, Y.; Wang, Z.; Müllen, K. *J. Am. Chem. Soc.* **2006**, *128*, 1334.
(91) Tang, C.; Tracz, A.; Kruk, M.; Zhang, R.; Smilgies, D.-M.; Matyjaszewski, K.; Kowalewski, T. *J. Am. Chem. Soc.* **2005**, *127*, 6918.
(92) Duffy, C. M.; Andreasen, J. W.; Breiby, D. W.; Nielsen, M. M.; Ando, M.; Minakata, T.; Sirringhaus, H. *Chem. Mater.* **2008**, *20*, 7252.
(93) Miskiewicz, P.; Mas-Torrent, M.; Jung, J.; Kotarba, S.; Glowacki, I.; Gomar-Nadal, E.; Amabilino, D. B.; Veciana, J.; Krause, B.; Carbone, D.; Rovira, C.; Ulanski, J. *Chem. Mater.* **2006**, *18*, 4724.
(94) Pisula, W.; Tomović, Ž.; Stepputat, M.; Kolb, U.; Pakula, T.; Müllen, K. *Chem. Mater.* **2005**, *17*, 2641.
(95) Tracz, A.; Jeszka, J. K.; Watson, M.; Pisula, W.; Müllen, K.; Pakula, T. *J. Am. Chem. Soc.* **2003**, *125*, 1682.
(96) Breiby, D. W.; Bunk, O.; Pisula, W.; Solling, T. I.; Tracz, A.; Pakula, T.; Müllen, K.; Nielsen, M. M. *J. Am. Chem. Soc.* **2005**, *127*, 11288.
(97) Breiby, D. W.; Hansteen, F.; Pisula, W.; Bunk, O.; Kolb, U.; Andreasen, J. W.; Müllen, K.; Nielsen, M. M. *J. Phys. Chem. B* **2005**, *109*, 22319.
(98) Piris, J.; Pisula, W.; Tracz, A.; Pakula, T.; Müllen, K.; Warman, J. M. *Liq. Cryst.* **2004**, *31*, 993.
(99) Piris, J.; Debije, M. G.; Stutzmann, N.; Laursen, B. W.; Pisula, W.; Watson, M. D.; Bjørnholm, T.; Müllen, K.; Warman, J. M. *Adv. Funct. Mater.* **2004**, *14*, 1053.
(100) Tsao, H. N.; Räder, H. J.; Pisula, W.; Rouhanipour, A.; Müllen, K. *Phys. Status Solidi A* **2008**, *205*, 421.
(101) Boamfa, M. I.; Viertler, K.; Wewerka, A.; Stelzer, F.; Christianen, P. C. M.; Maan, J. C. Phys. Rev. Lett. **2003**, *90*, Art. No. 025501.
(102) Lee, J.-H.; Choi, S.-M.; Pate, B. D.; Chisholm, M. H.; Han, Y.-S. *J. Mater. Chem.* **2006**, *16*, 2785.
(103) Shklyarevskiy, I. O.; Jonkheijm, P.; Stutzmann, N.; Wasserberg, D.; Wondergem, H. J.; Christianen, P. C. M.; Schenning, A. P. H. J.; de Leeuw, D. M.; Tomovic, Z.; Wu, J.; Müllen, K.; Maan, J. C. *J. Am. Chem. Soc.* **2005**, *127*, 16233.
(104) van de Craats, A. M.; Stutzmann, N.; Bunk, O.; Nielsen, M. M.; Watson, M.; Müllen, K.; Chanzy, H. D.; Sirringhaus, H.; Friend, R. H. *Adv. Mater.* **2003**, *15*, 495.
(105) Zimmermann, S.; Wendorff, J. H.; Weder, C. *Chem. Mater.* **2002**, *14*, 2218.
(106) Piris, J.; Debije, M. G.; Stutzmann, N.; van de Craats, A. M.; Watson, M. D.; Müllen, K.; Warman, J. M. *Adv. Mater.* **2003**, *15*, 1736.
(107) Bunk, O.; Nielsen, M. M.; Solling, T. I.; van de Craats, A. M.; Stutzmann, N. *J. Am. Chem. Soc.* **2003**, *125*, 2252.
(108) Brabec, C. J.; Sariciftci, N. S.; Hummelen, J. C. *Adv. Funct. Mater.* **2001**, *11*, 15.
(109) Mayer, A. C.; Scully, S. R.; Hardin, B. E.; Rowell, M. W.; McGehee, M. D. *Mater. Today* **2007**, *10*, 28.
(110) Schmidt-Mende, L.; Fechtenkötter, A.; Müllen, K.; Moons, E.; Friend, R. H.; MacKenzie, J. D. *Science* **2001**, *293*, 1119.
(111) Li, J.; Kastler, M.; Pisula, W.; Robertson, J. W. F.; Wasserfallen, D.; Grimsdale, A. C.; Wu, J.; Müllen, K. *Adv. Funct. Mater.* **2007**, *17*, 2528.
(112) Pisula, W.; Kastler, M.; Wasserfallen, D.; Robertson, J. W. F.; Nolde, F.; Kohl, C.; Müllen, K. *Angew. Chem., Int. Ed.* **2006**, *45*, 819.
(113) Wong, W. W. H.; Jones, D. J.; Yan, C.; Watkins, S. E.; King, S.; Haque, S. A.; Wen, X.; Ghiggino, K. P.; Holmes, A. B. *Org. Lett.* **2009**, *11*, 975.
(114) Wong, W. W. H.; Singh, T. B.; Vak, D.; Pisula, W.; Yan, C.; Feng, X.; Williams, E. L.; Chan, K. L.; Mao, Q.; Jones, D. J.; Ma, C.-Q.; Müllen, K.; Bäuerle, P.; Holmes, A. B. *Adv. Funct. Mater.* **2010**, *20*, 927.
(115) Mishra, A.; Ma, C.-Q.; Bäuerle, P. *Chem. Rev.* **2009**, *109*, 1141.
(116) Wong, W. W. H.; Ma, C.-Q.; Pisula, W.; Yan, C.; Feng, X.; Jones, D. J.; Müllen, K.; Janssen, R. A. J.; Bäuerle, P.; Holmes, A. B. *Chem. Mater.* **2010**, *22*, 457.
(117) Thiebaut, O.; Bock, H.; Grelet, E. *J. Am. Chem. Soc.* **2010**, *132*, 6886.
(118) Mathijssen, S. G. J.; Smits, E. C. P.; van Hal, P. A.; Wondergem, H. J.; Ponomarenko, S. A.; Moser, A.; Resel, R.; Bobbert, P. A.; Kemerink, M.; Janssen, R. A. J.; de Leeuw, D. M. *Nat. Nanotechnol.* **2009**, *4*, 674.